

A Spatio-Temporal Dirichlet Process Mixture Model on Linear Networks for Crime Data

Sujeong Lee¹, Won Chang³, Jorge Mateu⁴, Heejin Lee⁵, and Jaewoo Park^{*1,2}

¹Department of Statistics and Data Science, Yonsei University, Seoul, Republic of Korea.

²Department of Applied Statistics, Yonsei University, Seoul, Republic of Korea.

³Department of Statistics, Seoul National University, Seoul, Republic of Korea.

⁴Department of Mathematics, University Jaume I, Castellón, Spain.

⁵Department of Criminal Justice and Criminology, Sam Houston State University, Huntsville, USA.

January 21, 2026

Abstract

Analyzing crime events is crucial to understand crime dynamics and it is largely helpful for constructing prevention policies. Point processes specified on linear networks can provide a more accurate description of crime incidents by considering the geometry of the city. We propose a spatio-temporal Dirichlet process mixture model on a linear network to analyze crime events in Valencia, Spain. We propose a Bayesian hierarchical model with a Dirichlet process prior to automatically detect space-time clusters of the events and adopt a convolution kernel estimator to account for the network structure in the city. From the fitted model, we provide crime hotspot visualizations that can inform social interventions to prevent crime

*Corresponding Author: Jaewoo Park, Department of Statistics and Data Science, Yonsei University; Department of Applied Statistics, Yonsei University, Seoul, 03722, Republic of Korea (e-mail: jwpark88@yonsei.ac.kr)

incidents. Furthermore, we study the relationships between the detected cluster centers and the city’s amenities, which provides an intuitive explanation of criminal contagion.

Keywords: crime data, Dirichlet process, linear network, Markov chain Monte Carlo, spatio-temporal point processes

1 Introduction

Research in criminology has shown that crime spreads as a contagious disease in local areas (Johnson, 2008a; Mohler et al., 2011), with contagion rates varying between different types of crimes (Brantingham et al., 2021a,b). The spread of crime dynamics in urban areas shows complex patterns due to the geographical structure of the city (Brantingham et al., 2009; Dong et al., 2024; Song et al., 2013). Therefore, considering the geographical structure can help us better understand crime dynamics, predict future incidents more accurately, and effectively develop prevention strategies. In this manuscript, we study the space-time locations of crime events in Valencia, Spain, recorded from 2018 to 2019, considering the city’s road network structure. By using the exact space-time locations of crime events, we propose a novel spatio-temporal point process model that can understand the clustering patterns of the events.

Point process models have been proposed to understand the clustering behavior of crime events. In this context, spatio-temporal Hawkes process models (Park et al., 2021; Reinhart, 2018; Zhuang and Mateu, 2019) can capture clustering and triggering patterns by modeling the intensity through the past history of the process. Loeffler and Flaxman (2018) developed a self-exciting spatio-temporal point process to model gun violence, analyzing diffusion and clustering by estimating spatial and temporal intensities. Bayesian inference was performed using an efficient Hamiltonian Monte Carlo method. Lima (2023) provides a comprehensive review of Hawkes point processes and their applications. Multivariate point processes have also been studied to model different crime types. Hessellund et al. (2022) developed a semiparametric regression model for the intensity function that depends on an unspecified factor common to all crime types. Briz-Redón and Mateu (2023) introduced a mechanistic bivariate spatio-temporal model to study the intensity of two crime types. Mohler (2014) proposed a marked point process model for multiple crime types, which can capture both short-term and long-term hotspots. However, these

approaches have limited applicability to our particular data and motivating problem because they do not consider the road network structure. Our crime data can be naturally spatially inhomogeneous due to the network geometry, which additionally poses a significant challenge over classical spatio-temporal point process models. Specifically, if we do not consider the network structure, the places inaccessible to people could also be considered in the analysis. Furthermore, even if the two points are closely located in terms of Euclidean distances, the distance over the roads can be different depending on the network structure. Without considering such geometric structure, there can be non-negligible biases in the statistical inference.

There is a growing literature on computational methods for point processes on linear networks (see Baddeley et al. (2021) for a comprehensive review). Kernel density estimation methods have already been developed, such as the heat kernel (McSwiggan et al., 2017) that uses the density of a Brownian motion on the network. Rakshit et al. (2019b) proposed a convolution kernel estimator using a fast Fourier transformation. Moradi and Mateu (2020) developed summary statistics for point processes on a linear network, including the K-function and pair correlation function. D’Angelo et al. (2023) studied the local version of inhomogeneous second-order statistics for spatio-temporal point processes. Rakshit et al. (2019a) developed a memory-efficient algorithm to compute second-order summary functions of point patterns on a linear network. Recently, in a more complex setting where marks are associated with each event, Eckardt and Moradi (2024) developed summary statistics for various types of marks, including functional marks.

Although these previous works are useful for exploratory analysis, they do not employ model-based approaches. Developing point process models on road networks still remains challenging due to computational and inferential complexities. Recently, several spatio-temporal point process models have been studied in the context of linear networks. D’Angelo et al. (2022) proposed Gibbs point processes and log-Gaussian Cox processes to study the patterns of visitor stops by touristic attractions. D’Angelo et al. (2024) also developed spatio-temporal Hawkes point process models by including the network geometry in the inference procedure. They show that the proposed model fits much better compared to the planar one (Zhuang and Mateu, 2019). Gilardi et al. (2024) developed a non-separable intensity function to model ambulance interventions on road networks. Apart from these contributions, no further model-based strategies have been proposed.

Although these approaches can describe spatio-temporal patterns of the process defined over

linear networks, it is not trivial to detect the space-time clustering structure of crime events. Furthermore, fully Bayesian approaches have been under-explored. Such methods offer a natural framework for quantifying uncertainties within complex hierarchical models. A spatio-temporal point process typically has a hierarchical structure in which the observed process is modeled conditional on a latent process, and the latent process is modeled conditional on the model parameters (Cressie and Wikle, 2011). Frequentist approaches typically estimate the model parameters first and then plug in these estimates to infer the latent process, ignoring parameter estimation uncertainty. This can underestimate standard errors, which becomes more severe as the latent structure becomes more complex. On the other hand, Bayesian methods construct a joint posterior of the parameters and the latent process. By drawing samples from this joint posterior, parameter and latent uncertainties are fully propagated.

In this line, we propose a spatio-temporal Dirichlet process (DP) mixture model to analyze crime events that occurred in the road network of the city. DP mixture models have been widely applied across various disciplines—for instance, to estimate the intensities of tree locations (Kottas and Sansó, 2007), to model crime patterns (Taddy, 2010), to cluster population genetic data (Reich and Bondell, 2011), to model joint species distribution in ecology (Taylor-Rodríguez et al., 2017), and to detect disease hotspots (Park et al., 2023).

The main contributions of the manuscript are as follows. This study is the first attempt to develop a spatio-temporal DP point process on a linear network. Our model can automatically choose the number and location of cluster centers of crime events. To account for the structure of the linear network in the city, we adopt the convolution kernel estimator (Rakshit et al., 2019b), which can be quickly computed using the fast Fourier transformation. Second, we develop a fully Bayesian inference framework for the proposed model, enabling flexible hierarchical modeling and proper uncertainty quantification via posterior samples. Notably, most previous studies on point processes over linear networks have focused on exploratory analyses (Rakshit et al., 2019a; Baddeley et al., 2021; Eckardt and Moradi, 2024), rather than formal statistical inference. Lastly, we introduce a model assessment approach that compares the empirical and theoretical proportions of events based on the likelihood function. We show that the proposed model more effectively captures spatio-temporal patterns in the crime data compared to the classical DP model.

With the proposed model, we analyzed two types of crime events—robbery and theft—recorded

in Valencia from 2018 to 2019. Our main findings can be summarized as follows. First, crime clusters (i.e., hotspots) tend to influence within a spatial radius of approximately $1.1km$ and a temporal window of about seven months. Furthermore, both robbery and theft exhibit peaks during the summer and fall seasons. Second, we observe that crime intensities are correlated with commercial areas, which tend to attract criminal activities. In addition, crimes are concentrated in urban, densely populated regions, whereas they are relatively rare in rural areas. Lastly, robbery and theft hotspots show an attractive tendency during peak periods. Moreover, theft occurrences have a positive effect on robbery and exhibit significant spatio-temporal auto-correlation.

The outline of the remainder of this paper is as follows. In Section 2, we describe the crime events data in Valencia, Spain. We also provide an exploratory data analysis for the dataset. In Section 3, we propose a spatio-temporal DP mixture model on a linear network and describe details about model inference. In Section 4, we apply our method to real crime data, illustrating that our model can capture the spatio-temporal cluster centers of crime events. In addition, we study the relationship between cluster centers and the amenities of the city, which provides important sociological interpretations. In Section 5, we conclude the paper with a summary and some further discussion.

2 Data description and exploratory analysis

The dynamics of crime contagion are particularly complex within urban settings, influenced heavily by the geographic layout of the city. While crimes occur in a continuous space (*e.g.*, within a city area measured by longitude and latitude), they are mostly confined to the street networks, influencing both the escape routes of criminals and the spatial distribution of crime. Early research also suggests that crime's contagious effects propagate along these street networks instead of dispersing freely, as evidenced by a fitted non-parametric influence kernel from real crime events. Motivated by these facts, in this section, we describe our crime data and provide some first exploratory data analysis.

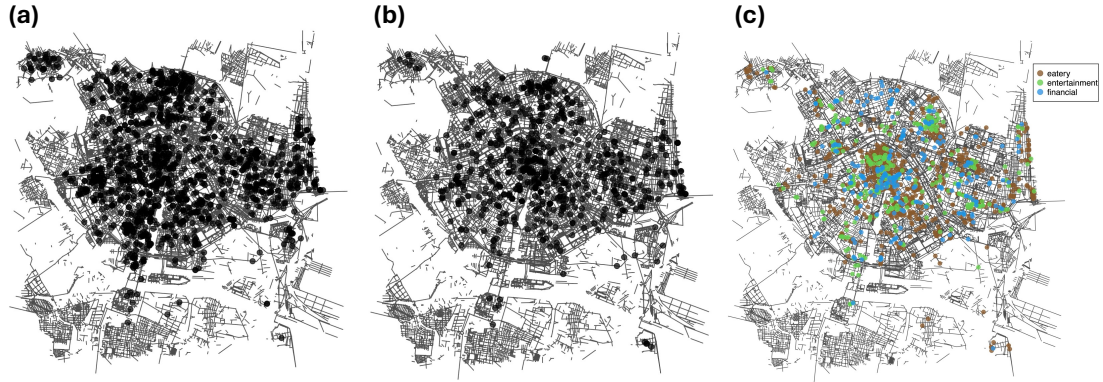


Figure 1: Locations of (a) robbery incidences, (b) theft incidences, and (c) amenities.

2.1 Data: crime events in Valencia, Spain

Valencia is a city on the Mediterranean coastline that has a population of more than 1.5 million (Dong et al., 2024). The crime data in this study is collected by the local police department in Valencia (Spain) and records the exact location and time for each crime event, allowing us to use the framework of spatio-temporal point processes. The raw dataset comprises four categories of crime: robbery, theft, alarms related to women, and other offenses. Robbery and theft are frequently examined in criminology due to their clear legal definitions and the substantial social harm they entail. For these reasons, we also focus on these two types of crime in our study. Robbery refers to the taking of property through force or threat, whereas theft involves the unlawful taking of property without consent. These definitions render both offenses more amenable to operationalization and measurement in crime statistics than more ambiguous or less detectable crimes (e.g., drug use, alcoholism, prostitution). Moreover, theft ranks among the most prevalent offenses globally (van Dijk et al., 2022). Accordingly, robbery and theft are often employed in criminological research to test and refine theoretical frameworks, particularly those addressing property crime (Chastain et al., 2016; Groff, 2007; Johnson, 2008b). While robbery and theft may be linked to similar criminal opportunities (e.g., availability of suitable targets), resulting in overlapping geographical patterns, the two crimes are distinct—differing in the presence of violence, the level of risk to victims, and the situational dynamics under which they occur—and are therefore studied separately. Figure 1a and 1b depicts the locations of these two crimes in the city. In our analysis, we used observations within 500 meters of each single

street and projected them on the closest street, resulting in 1,423 records of robbery and 699 records of theft from 2018-01-01 to 2019-12-31 in the city of Valencia (Spain). We describe further details of the street network in Section 2.2. We observe that the spatial patterns of both crimes are quite similar, occurring mainly towards downtown rather than in the outskirts of the city, with lots of variations in both the degree of the vertices and the lengths of the streets.

In addition to crime events, to investigate the relationship between the patterns of the reported crimes and the surrounding urban environment, we also have the geographical locations of different amenities in Valencia, including ATMs, banks, bars, cafes, nightclubs, pubs, and restaurants. In our study, we categorize the amenities into three groups: (a) entertainment (bars, nightclubs, pubs, with 286 amenities), (b) financial (ATMs, banks, with 246 amenities), and (c) eatery (cafes, restaurants, with 940 amenities). Figure 1c illustrates the locations of these amenities in the city.

2.2 Exploratory data analysis

Here, we set some background for point patterns on networks while providing some motivation for a cluster point process model. Consider a linear network $\mathcal{L} = \bigcup_{i=1}^n l_i \subseteq \mathbb{R}^2$, as a finite union of line segments $l_i \subseteq \mathbb{R}^2$ (Baddeley et al., 2021). The line segments are defined as $l_i = [u_i, v_i] = \{ku_i + (1-k)v_i : 0 \leq k \leq 1\}$, where $u_i, v_i \in \mathbb{R}^2$ are the endpoints of l_i . For $i \neq j$, the intersection of l_i and l_j is empty or an endpoint of both segments. When considering a time domain $\mathcal{T} \subseteq \mathbb{R}^+$, we can introduce a spatio-temporal point process \mathbf{X} over the bounded domain $\mathcal{L} \times \mathcal{T}$. This process thus contains information about the space-time locations for the crime events.

We first convert Valencia’s street network as a spatial object using `osmdata` (Mark Padgham et al., 2017) package in R. We can then represent the data through a projected coordinate reference system (EPSG code: 2062) of Spain that measures units in meters. Specifically, we select all the road features inside a rectangular window (with width 11.3km and height 12.59km) defined by spatial coordinates, including the Valencia border. Then, we convert the data into a linear network format (i.e., `linnet` object in `spatstat.linnet` package). The linear network of Valencia inside a rectangular window contains 49,251 vertices (nodes) and 37,490 line segments (edges). However, using all line segments in the analysis is impractical because street crime events

rarely occur on certain road types (e.g., highways), and analyzing the large network would involve high memory usage and computation cost. Therefore, we chose such streets where crime events could potentially occur, including residential streets, living streets, pedestrian streets, footways, service streets, steps, corridors, sidewalks, crossings, and cycleways. Residential streets serve as access to housing. Living streets are residential areas where pedestrians are legally prioritized, and vehicle speeds are strictly restricted. Footways are designated pathways primarily intended for pedestrian use. Service streets are roads within or leading to areas like alleys and business parks. Corridors are hallways within buildings. Following this procedure, we finally obtained a linear network consisting of 44,018 vertices (nodes) and 31,553 line segments (edges) with a width of $10.562km$ and a height of $10.745km$, referring to Valencia, whose total length of all line segments is about $1,992km$.

To understand the pattern of both types of crime events, we first compute first-order spatial intensities (depicted in Figure 2) by using the convolution kernel estimator (Rakshit et al., 2019b) that accounts for the street structure. We use Scott’s rule (Scott, 2015) to select the bandwidth for kernel density estimation. Figure 2 illustrates that robbery crime events show higher intensity values in the top and bottom areas of the city, while theft crime events are more concentrated in the center of the city. These findings are aligned with Figure 1.

We compute the linear network K -function (Moradi and Mateu, 2020) to study second-order characteristics of the point patterns. Specifically, the K -function is defined as

$$K_{LI}^{ST}(r, t) = \mathbb{E} \left[\sum_{(\mathbf{x}, t_x) \in X} \frac{\mathbb{1}\{0 < d_{\mathcal{L}}(\mathbf{u}, \mathbf{x}) < r, |t_u - t_x| < t\}}{\lambda(\mathbf{x}, t_x)M((\mathbf{u}, t_u), d_{\mathcal{L}}(\mathbf{u}, \mathbf{x}), |t_u - t_x|)} | (\mathbf{u}, t_u) \in X \right], \quad (1)$$

where $\lambda(\mathbf{x}, t_x)$ is the first-order intensity and $M((\mathbf{u}, t_u), r, t)$ is the number of points lying exactly at the shortest-path distance r and the time distance t away from (\mathbf{u}, t_u) . In (1), $d_{\mathcal{L}}(\mathbf{u}, \mathbf{x})$ is shortest distance between \mathbf{u} and \mathbf{x} and $|\cdot|$ is the Euclidean distance. The K -function (Ripley, 1976) has been widely used to assess whether a point pattern exhibits clustering, regularity, or complete spatial randomness. Specifically, point patterns are repeatedly simulated under a null model (i.e., complete spatial randomness), and the K -function is computed for each simulation. The K -function derived from the observed data is then compared to the range of simulated K -functions to detect significant deviations from the null hypothesis. This procedure is referred to

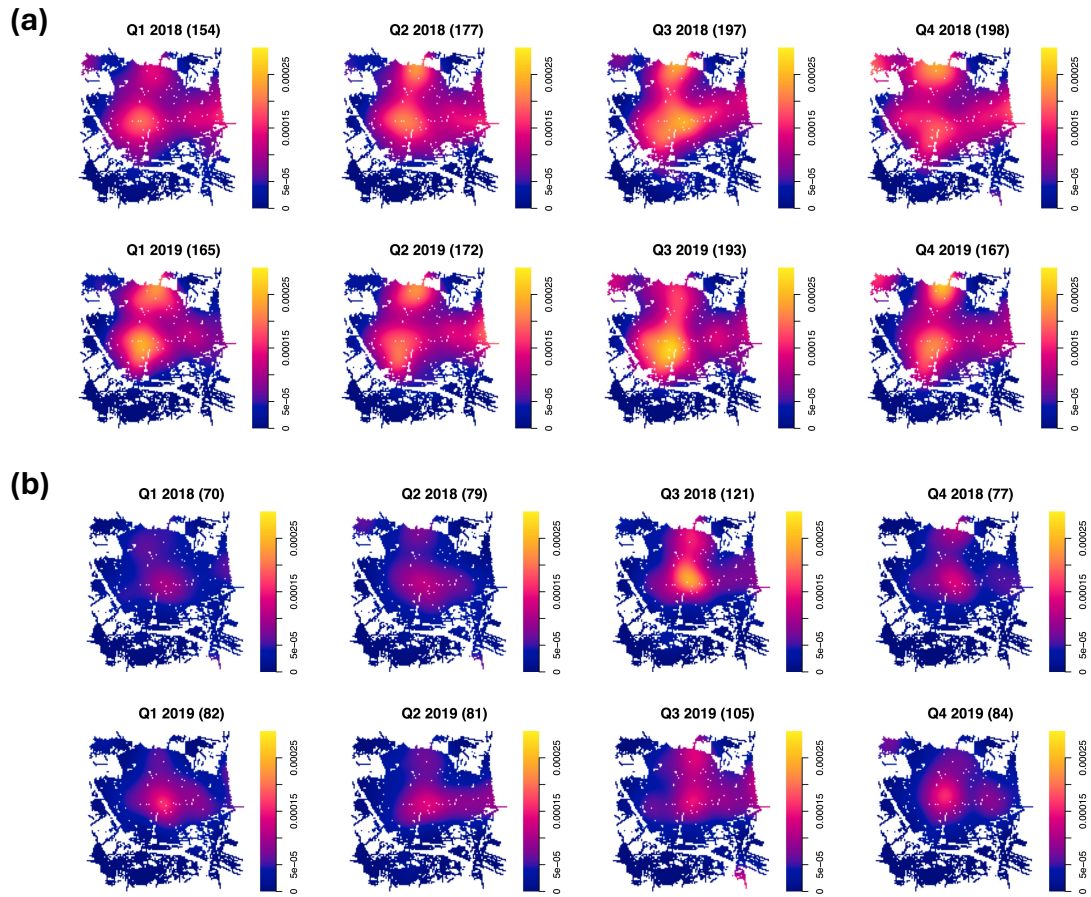
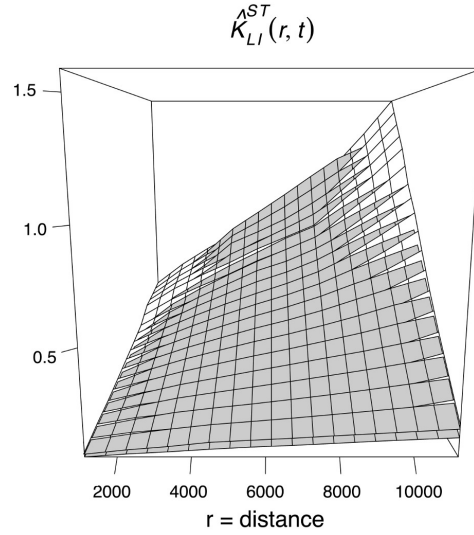
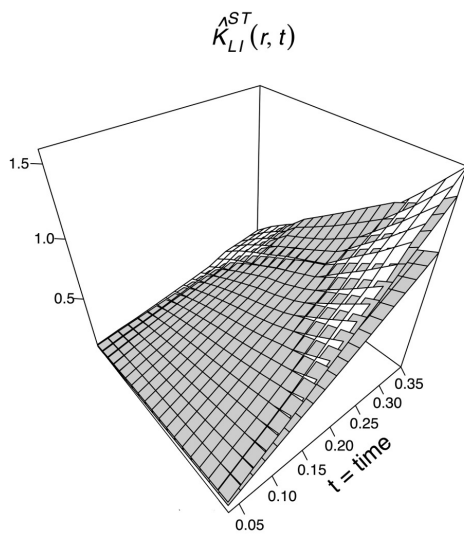


Figure 2: Estimated first-order spatial intensity of (a) robbery and (b) theft by quarters and corresponding crime counts in the parentheses.

(a)



(b)

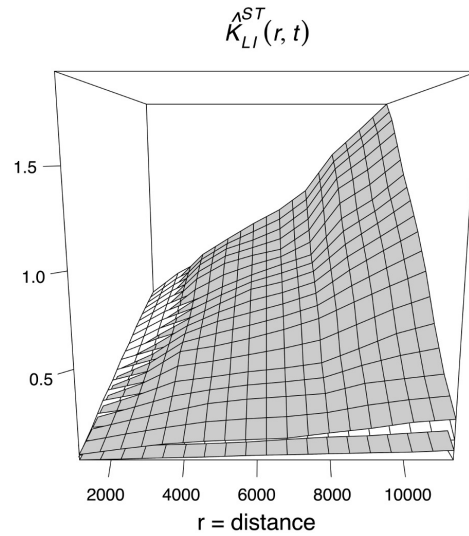
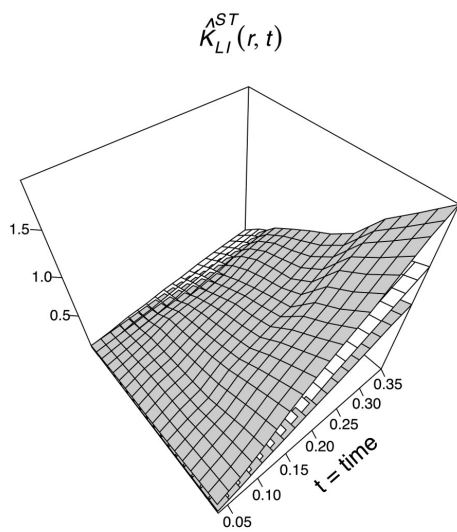


Figure 3: Estimated K -functions for (a) robbery and (b) theft, illustrated over time and distance dimensions. Gray colors are simulation envelopes generated from homogeneous Poisson processes, with the lower surface representing the minimum and the upper one representing the maximum K -functions. White colors indicate K -functions from the observed crime data. Areas where the observed K -function exceeds the simulation envelopes are highlighted in white.

as constructing simulation envelopes. In our study, we first compute a nonparametric estimate of the K -function (Moradi and Mateu, 2020), $\hat{K}_{LI}^{ST}(r, t)$ from the observed point patterns. We then generate K -functions from 99 simulated homogeneous Poisson processes (i.e., the null model). When the observed K -function exceeds the simulation envelopes, it indicates significant clustering at the corresponding spatial and temporal scales. Figure 3 shows that crime events—both robbery and theft—exhibit clustering within a temporal range of 0.2 to 0.35 (approximately 5 to 8 months) and at spatial distances below 4,000 meters. In addition, robbery displays a notable clustering pattern at a temporal lag of around 0.15 (approximately 3 months) and at spatial distances exceeding 8,000 meters. Following Moradi and Mateu (2020), we also compute a p-value to test the null hypothesis of Poissonness (absence of any sort of clustering), defined as

$$T = \int \int \frac{\hat{K}_{LI}^{ST}(r, t) - E_K(r, t)}{\sqrt{V_K(r, t)}} dr dt,$$

$$\text{p-value} = \frac{1 + \sum_{i=1}^m \mathbb{1}\{T_i > T^*\}}{m + 1}, \quad (2)$$

where E_K and V_K are the mean and variance of $\hat{K}_{LI}^{ST}(r, t)$. In (2), each T_i is computed from a simulated point pattern generated from a homogeneous Poisson process (i.e., null hypothesis), and T^* is computed from the observed point pattern. The p-values for robbery and theft were 0.02 and 0.04, respectively; therefore, we can conclude that the crime events are not compatible with a homogeneous spatio-temporal Poisson process and, indeed, highlight structures with varying clustering degrees.

3 A Dirichlet process mixture model on a linear network

We propose and develop a spatio-temporal DP mixture model considering the geometrical structure of the linear network. The method can detect unobserved cluster centers of street crimes and underpin hotspots.

3.1 Model framework

Let $\{(\mathbf{x}_i, t_i)\}_{i=1}^N$ be a realization of the point process \mathbf{X} over the bounded domain $\mathcal{L} \times \mathcal{T}$. We consider the space domain over the linear network $\mathcal{L} \in \mathbb{R}^2$, and a normalized time domain $\mathcal{T} = [0, 1]$. Normalizing the time domain has several practical advantages and is commonly adopted in spatio-temporal point process analysis (Møller and Waagepetersen, 2003; Baddeley et al., 2015). First, the normalization removes the influence of specific time units (e.g., weeks, months, years) on model fitting, allowing for consistent interpretation of model results across different temporal scales. Furthermore, rescaling the temporal domain can improve the computational stability of MCMC algorithms. In our problem, each (\mathbf{x}_i, t_i) denotes the location and time of a crime event. We introduce the latent space-time cluster centers as $\mathbf{c} = \{(\mathbf{c}_j^s, c_j^t)\}_{j=1}^M \in \mathcal{L} \times \mathcal{T}$. To assign an i th observation to a cluster, we define the cluster membership variable $g_i \in \{1, \dots, M\}$ and model the membership variable as a DP prior (Ishwaran and James, 2001). Specifically, we model a g_i as

$$g_i \sim \text{Categorical}(q_1, \dots, q_M),$$

where q_1, \dots, q_M represents the cluster probabilities for crime events. Then we model the cluster membership probabilities as the stick-breaking process prior (Sethuraman, 1994):

$$q_j = \begin{cases} U_1, & \text{for } j = 1 \\ U_j \prod_{m=1}^{j-1} (1 - U_m), & \text{for } j = 2, \dots, M, \end{cases} \quad (3)$$

where $U_1, \dots, U_m \stackrel{\text{iid}}{\sim} \text{Beta}(1, b_u)$ with rate parameter b_u . In our analysis, we set a hyperprior for b_u as $\text{Gamma}(1, 1)$ and $\text{Gamma}(1, 1/4)$, following Reich and Bondell (2011). Note that b_u controls the expected number of clusters. This choice can encourage the number of non-empty clusters to lie between 1 and 15, thereby allowing the regularization to reduce the possibility of overfitting. In the stick-breaking process prior, the initial mixture probability q_1 is represented as a beta random variable U_1 . For $j = 2, \dots, M$, the subsequent mixture probabilities q_j are obtained by multiplying $1 - \sum_{m=1}^{j-1} q_m$, the remaining probability, with U_j , the proportion assigned to the j th cluster component. Theoretically, (3) considers an infinite number of clusters. However,

in practice, we approximate it with a sufficiently large $M < \infty$. The remaining probabilities $1 - \sum_{m=1}^{j-1} q_m$ become 0 for large j ; therefore, no observation is assigned to the j th cluster. From this finite representation, we can automatically choose the number of non-empty cluster centers.

After we assign the cluster membership to each observation, we model the space-time locations of crime events. Specifically, we define the conditional distribution for a given g_i as

$$f((\mathbf{x}_i, t_i) \mid g_i = j) \propto K_S(\mathbf{x}_i; \mathbf{c}_j^s, w_s) K_T(t_i; c_j^t, w_t), \quad (4)$$

where $K_S(\cdot)$ and $K_T(\cdot)$ are spatial and temporal kernels, respectively. In our study, we use $K_T(t_i; c_j^t, w_t)$ as a Gaussian kernel with center c_j^t and a standard deviation w_t (temporal range of cluster centers). There are several options for the spatial kernel $K_S(\cdot)$ that can account for the network geometry (see Baddeley et al. (2021) for a comprehensive review). One might consider the equal-split continuous kernel estimator (Okabe and Sugihara, 2012), which is a path enumeration method. At each fork in the linear network, the method divides the remaining tail mass at the vertex equally across the outgoing line segments. Therefore, the method can preserve the total mass. However, the implementation of the equal-split continuous kernel estimate is computationally demanding for large observations with complex street structures, as happens in our case. The heat kernel (McSwiggan et al., 2017), which exploits the connection between kernel smoothing and diffusion, can be another option. However, we observe that the heat kernel is not appropriate for our application because the computation time increases quadratically with increasing bandwidth. For practical implementation, we use the convolution kernel estimator (Rakshit et al., 2019b). This convolution kernel estimator of the intensity with Jones-Diggle correction is given by

$$K_S(\mathbf{x}_i; \mathbf{c}_j^s, w_s) = \frac{\kappa(\mathbf{x}_i; \mathbf{c}_j^s, w_s)}{c_{\mathcal{L}}(\mathbf{c}_j^s)}, \quad (5)$$

where $c_{\mathcal{L}}(\mathbf{c}_j^s) = \int_{\mathcal{L}} \kappa(\mathbf{v}; \mathbf{c}_j^s, w_s) d_1 \mathbf{v}$ is a correction term, and \mathbf{v} is an arbitrary point on \mathcal{L} . In (5), the numerator κ is a planar Gaussian kernel with a smoothing bandwidth w_s . Note that we can interpret it as a spatial range of clusters since the bandwidth is equivalent to the standard deviation of the Gaussian kernel (Chiu, 1991). The denominator in (5) is a convolution of the

kernel $\kappa(\cdot)$ with the arc-length measure on the network, and thus the kernel $K_S(\cdot)$ can account for the geometrical structure of the street network. In particular, the correction term $c_{\mathcal{L}}(\mathbf{c}_j^s)$ can be obtained through Monte Carlo integration

$$c_{\mathcal{L}}(\mathbf{c}_j^s) \approx \frac{|\mathcal{L}|}{N} \sum_{k=1}^N \kappa(\mathbf{v}_k; \mathbf{c}_j^s, w_s), \quad (6)$$

where $\mathbf{v}_1, \dots, \mathbf{v}_N$ are generated from \mathcal{L} , which is a uniform distribution over the linear network. In our case, we observe that $N = 1,000$ can provide an accurate Monte Carlo approximation.

We thus model the membership variable $g_i \sim \text{Categorical}(\tilde{q}_{i1}, \dots, \tilde{q}_{iM})$, where each \tilde{q}_{ij} is set as

$$\tilde{q}_{ij} \propto q_j K_S(\mathbf{x}_i; \mathbf{c}_j^s, w_s) K_T(t_i; c_j^t, w_t), \quad j = 1, \dots, M. \quad (7)$$

Equation (7) implies that it is likely that the i th observation is assigned to the j th cluster if (\mathbf{x}_i, t_i) is close to (\mathbf{c}_j^s, c_j^t) . In (3), we assign the stick-breaking prior for q_j , and this ensures only $M^* (< M)$ non-empty clusters. From the mixture model specified above, the full likelihood function is of the form

$$L(\boldsymbol{\theta} | \mathbf{X}, \mathbf{c}) \propto \prod_{i=1}^N \left[\sum_{\forall j \text{ non-empty}} q_j K_S(\mathbf{x}_i; \mathbf{c}_j^s, w_s) K_T(t_i; c_j^t, w_t) \right], \quad (8)$$

where $\boldsymbol{\theta} = (w_s, w_t)$ is a model parameter. With a prior specification, the joint posterior distribution can be formulated as $\pi(\boldsymbol{\theta}, \mathbf{c}, \{g_i\}_{i=1}^N, \{U_j\}_{j=1}^M, b_u | \mathbf{X})$. For w_s and w_t , we use flat truncated normal priors to ensure the positivity of the variances. Since the average length of each street in the entire Valencia is around $92.65m$ and points over $2km$ apart are considered distant for clustering, we set the lower and upper bounds for w_s as 100 and 1,000 metres, respectively. Here, we also consider the criminological literature, which widely uses a $150m \times 150m$ grid as a spatial unit (Block, 2000; Santitissadeekorn et al., 2018). This unit size reflects the largest area a single police officer typically covers on foot patrol within a designated beat (Zhang et al., 2022). For w_t , we set the lower bound of the prior as 0. For \mathbf{c} , we use the uniform prior defined over the network and the time period. To accelerate computation, we propose a spatial location of the

cluster center uniformly from the set of line segments Δ longer than $500m$. The hierarchical model structure and full conditionals for all components are described in the supplementary material. Algorithm 1 summarizes the Markov chain Monte Carlo (MCMC) procedure for Bayesian inference.

3.2 Post-Processing

Post-processing is required to obtain the final results from DP-based methods due to the label switching issue (see, *e.g.*, Medvedovic and Sivaganesan, 2002; Dahl, 2006; Reich and Bondell, 2011), where labels for any two different clusters can be swapping at a certain point of the MCMC chain. Without post-processing, each cluster label may represent multiple clusters in the data, leading to spurious multi-modality and overestimated variability. To address this, we identify the b^* th iteration of the MCMC chain that minimizes a loss related to cluster memberships, as follows:

$$b^* = \arg \min_b \left\{ \sum_{i=1}^N \sum_{j=1}^N \{ \mathbb{1}(g_i^b = g_j^b) - d_{ij} \}^2 \right\}, \quad d_{ij} = \sum_{b=1}^B \{ \mathbb{1}(g_i^b = g_j^b) / B \}$$

Here, B denotes the total number of iterations in the MCMC, and g_i^b denotes the membership of the sampled segment for the i th observation in the b th iteration. This solution minimizes the posterior expected loss for estimated segment membership proposed by Binder (1978) in Bayesian model-based clustering (Dahl, 2006).

3.3 Model assessment

We evaluate the performance of our model by comparing the empirical proportion of data points with the theoretical proportion derived from the likelihood function. Consider the rectangular cubes covering our spatio-temporal domain. The theoretical proportion corresponding to the cube $[\alpha_g, \beta_g]^3$ is calculated as

$$p_g^t = \int_{[\alpha_g, \beta_g]^3 \in \mathcal{L} \times \mathcal{T} \forall j \text{ non-empty}} \sum q_j K_S(\mathbf{x}; \mathbf{c}_j^s, w_s) K_T(t; c_j^t, w_t) d\mathbf{X},$$

where $\mathbf{X} \in \mathcal{L} \times \mathcal{T}$ represents the spatio-temporal point process. Since the integral in the above equation is analytically intractable, we compute an approximation, \hat{p}_g^t , through numerical inte-

Algorithm 1 MCMC algorithm for an STDP on a linear network

Given $\{\boldsymbol{\theta}^{(b)}, \mathbf{c}^{(b)}, \{g_i^{(b)}\}_{i=1}^N, \{U_j^{(b)}\}_{j=1}^M, b_u^{(b)}\}$ at the b -th iteration

Update the model parameters $\boldsymbol{\theta}^{(b+1)}$:

Propose $\boldsymbol{\theta}^* \sim q(\cdot|\boldsymbol{\theta}^{(b)})$ and accept $\boldsymbol{\theta}^{(b+1)} = \boldsymbol{\theta}^*$ with probability

$$\alpha = \min \left\{ 1, \frac{\pi(\boldsymbol{\theta}^*|\mathbf{c}^{(b)}, \{g_i^{(b)}\}_{i=1}^N, \{U_j^{(b)}\}_{j=1}^M, b_u^{(b)})}{\pi(\boldsymbol{\theta}^{(b)}|\mathbf{c}^{(b)}, \{g_i^{(b)}\}_{i=1}^N, \{U_j^{(b)}\}_{j=1}^M, b_u^{(b)})} \right\}$$

Update cluster index probability for each observation:

Generate $g_i^{(b+1)} \sim \text{Categorical}(\tilde{q}_{i1}, \dots, \tilde{q}_{iM})$, where

$$\tilde{q}_{ij} \propto q_j K_S(\mathbf{x}_i; \mathbf{c}_j^s, w_s) K_T(t_i; c_j^t, w_t)$$

for $i = 1, \dots, N$ and $j = 1, \dots, M$.

Update Dirichlet process parameters:

Generate

$$U_j^{(b+1)} \sim \text{Beta}\left(1 + \sum_{i=1}^N \mathbb{1}\{g_i^{(b+1)} = j\}, b_u^{(b)} + \sum_{i=1}^N \mathbb{1}\{g_i^{(b+1)} > j\}\right)$$

for $j = 1, \dots, M$.

Generate

$$b_u^{(b+1)} \sim \text{Gamma}\left(M, c - \sum_{j=1}^{M-1} \log(1 - U_j^{(b+1)})\right)$$

Update space-time cluster centers $\mathbf{c}^{(b+1)}$:

Propose $(\mathbf{c}_j^{s*}, c_j^{t*}) \sim \frac{1}{|\Delta|\mathcal{T}}$ and accept $(\mathbf{c}_j^{s(b+1)}, c_j^{t(b+1)}) = (\mathbf{c}_j^{s*}, c_j^{t*})$ with probability

$$\alpha = \min \left\{ 1, \frac{\pi((\mathbf{c}_j^{s*}, c_j^{t*})|\boldsymbol{\theta}^{(b+1)}, \{g_i^{(b+1)}\}_{i=1}^N, \{U_j^{(b+1)}\}_{j=1}^M, b_u^{(b+1)})}{\pi((\mathbf{c}_j^{s(b)}, c_j^{t(b)})|\boldsymbol{\theta}^{(b+1)}, \{g_i^{(b+1)}\}_{i=1}^N, \{U_j^{(b+1)}\}_{j=1}^M, b_u^{(b+1)})} \right\}$$

for $j = 1, \dots, M$.

gration. This is implemented with the `pmvnorm` function from the R package `mvtnorm`. Similarly, we compute the observed proportion of data points corresponding to the cube $[\alpha_g, \beta_g]^3$ as

$$p_g^o = \frac{\text{the number of observations in } [\alpha_g, \beta_g]^3}{\text{total number of observations}}.$$

We compare \hat{p}_g^t and p_g^o computed on each cube. Note that if we use too small cubes, we would have a lot of zeros for p_g^o because there will be no observation in $[\alpha_g, \beta_g]^3$. On the other hand, if we use too large cubes, the approximation error for \hat{p}_g^t becomes larger because the cubes will also cover the region without the roads. To address this, we first construct $G_s = 200 \times 200 \times 10$ number of subgrid points (i.e., high-resolution grid) over $\mathcal{L} \times \mathcal{T}$ and compute \hat{p}_g^t and p_g^o at each cube. Then, we aggregate them into larger, nonoverlapping grid points $G = 5 \times 5 \times 10$ that also cover $\mathcal{L} \times \mathcal{T}$. We provide details on grid computation in the supplementary material.

The proposed assessment method is related to residual analysis, which is commonly used for point process model validation (Baddeley et al., 2005). This approach also computes the discrepancies between observed proportions p_g^o and the estimated theoretical proportions \hat{p}_g^t to generate residual maps; residual values distributed around zero indicate a good model fit. Note that p_g^o and \hat{p}_g^t are the same quantities defined earlier in this section. We present the results in the supplementary material, where our model shows better agreement with the observed data compared to the standard DP model (Park et al., 2023).

4 Application

We applied our proposed method to the Valencia crime data described in Section 2.1. The code was implemented in R version 4.1.3 (R Core Team, 2022) and executed on an AMD Ryzen 9 5950X 16-core processor. The complete MCMC analysis, comprising 20,000 iterations and post-processing, required approximately 23 hours for crime type robbery, and 9 hours for crime type theft. The maximum number of clusters was set to 80 for robbery and 70 for theft, with the number of detected clusters automatically determined to be below these limits. Here, note that we need to penalize the maximum number of cluster centers. Setting the maximum number of clusters excessively high with small range parameters results in dense centers throughout the

region, leading to overfitting. However, if there are few centers, it may not detect centers in the area.

4.1 Crime hotspots

Figure 4 shows detected cluster centers and their offspring for each crime type, analyzed quarterly over the two-year period. Robbery cluster centers were more frequently detected in Q2 of 2018 and Q3 of 2019, while theft clusters were more commonly detected in Q3 of 2019. These findings align with prior research on seasonal variations in crime levels (Cohn, 1990; Farrell and Pease, 1994; McDowall et al., 2012). Numerous studies have demonstrated that both violent and property and personal crimes tend to peak during the summer or fall months (Deckard and Schnell, 2023; Haberman et al., 2018; Hipp et al., 2004; Kim and Wo, 2022). This pattern is likely attributable to shifts in individuals' routine activities, such as vacation and outdoor events, which increase the likelihood of convergence between potential offenders and suitable victims in the absence of effective guardianship (Cohen and Felson, 1979). Additional evidence supporting this argument is the peak in tourist numbers in Valencia between May and October (Q2 and Q3) in both 2018 and 2019 (Instituto Nacional de Estadística, 2025).

Figure 5 represents the posterior mean of the density on the linear network, calculated by our model (8), with the estimated range parameter plugged in. We observe that areas with higher observed counts correspond well to regions of higher posterior means, indicating a good model fit. This figure shows robbery highlighted in yellow in the upper area in Q2 of 2018 and the bottom area in Q3 of both years. For theft, the number of detected cluster centers is smaller than that for robbery, with a denser concentration in Q3 of both years. Interestingly, the patterns of robbery and theft exhibit similarities in the right side in Q2 and Q3 of 2019. For both crime types, hotspots appear to be shifting from one quarter to the next. This observation supports the literature indicating that hotspots exhibit short-term stability, typically lasting only a few months (Deckard and Schnell, 2023; Groff et al., 2015). Consequently, focusing police and social service resources in crime hotspots for brief periods may be effective in achieving notable reductions in crime (Weisburd, 2018).

To assess model fitting, we compare our proposed model with the standard spatio-temporal

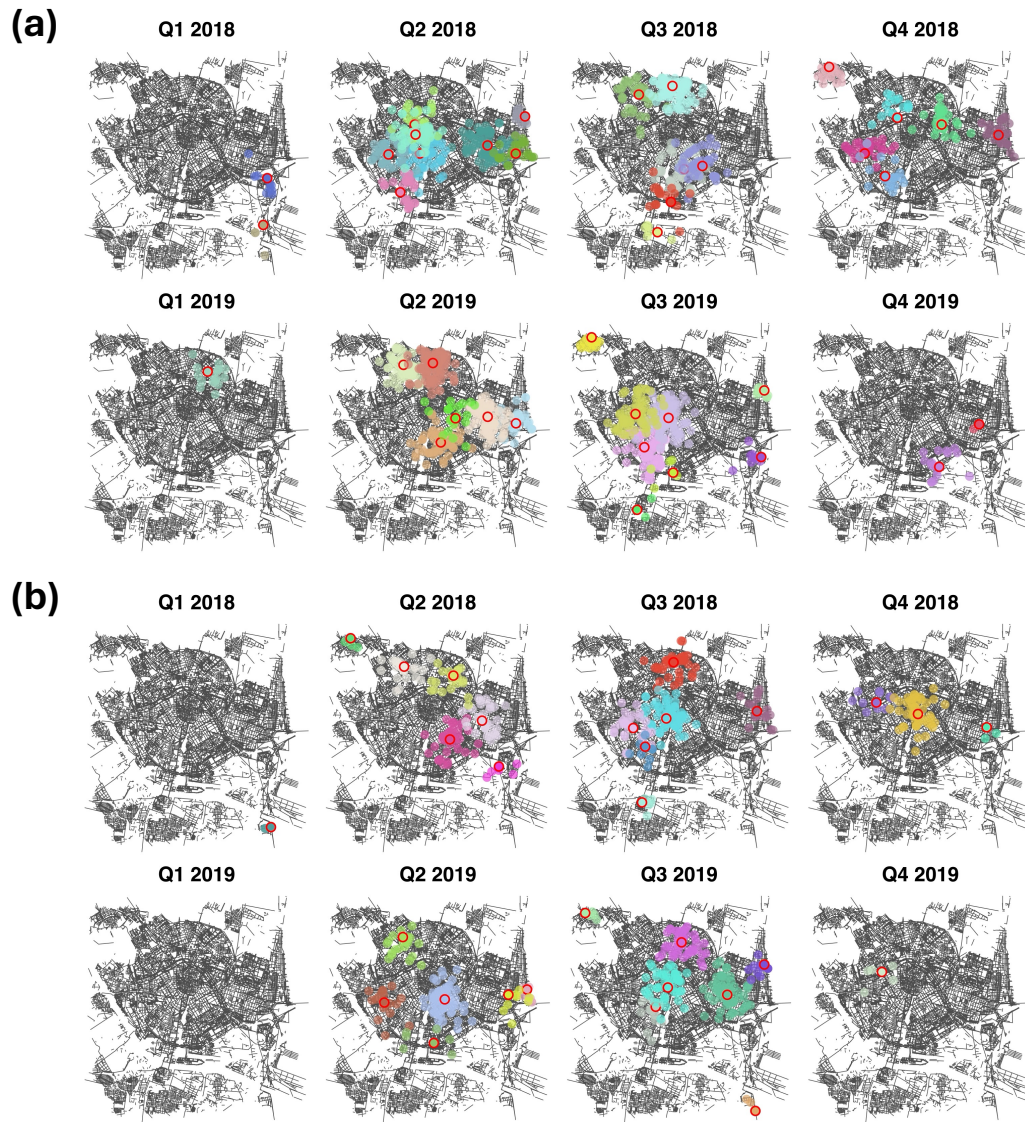


Figure 4: Detected cluster centers and their offspring by quarters of (a) robbery and (b) theft. The red-outlined dots indicate detected cluster centers, while the surrounding dots of the same color represent their offspring belonging to the same cluster.

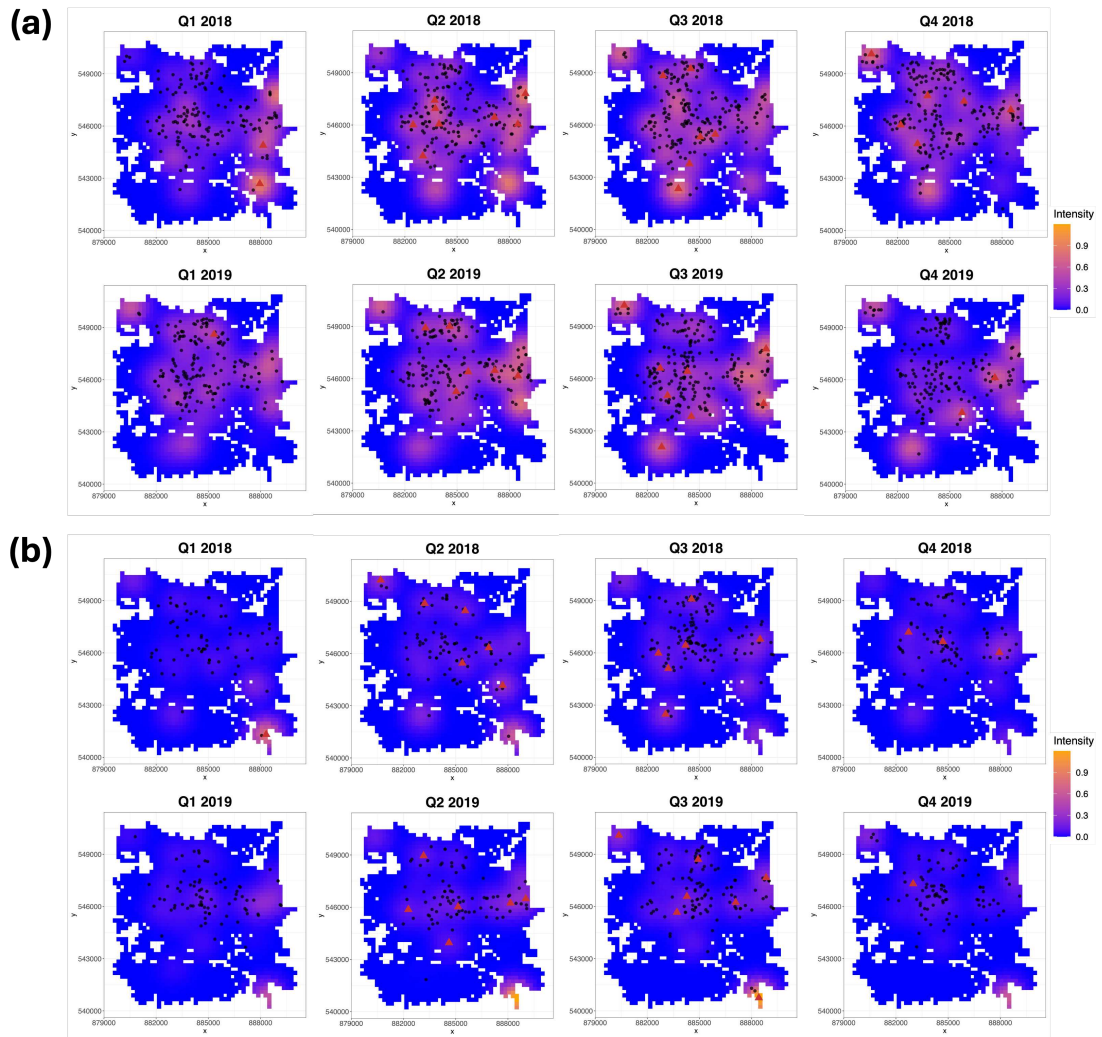


Figure 5: Posterior means of the density of the observed cases of (a) robbery and (b) theft by quarter. Black dots represent the observed crime events during each period, while red triangles indicate the detected cluster centers.

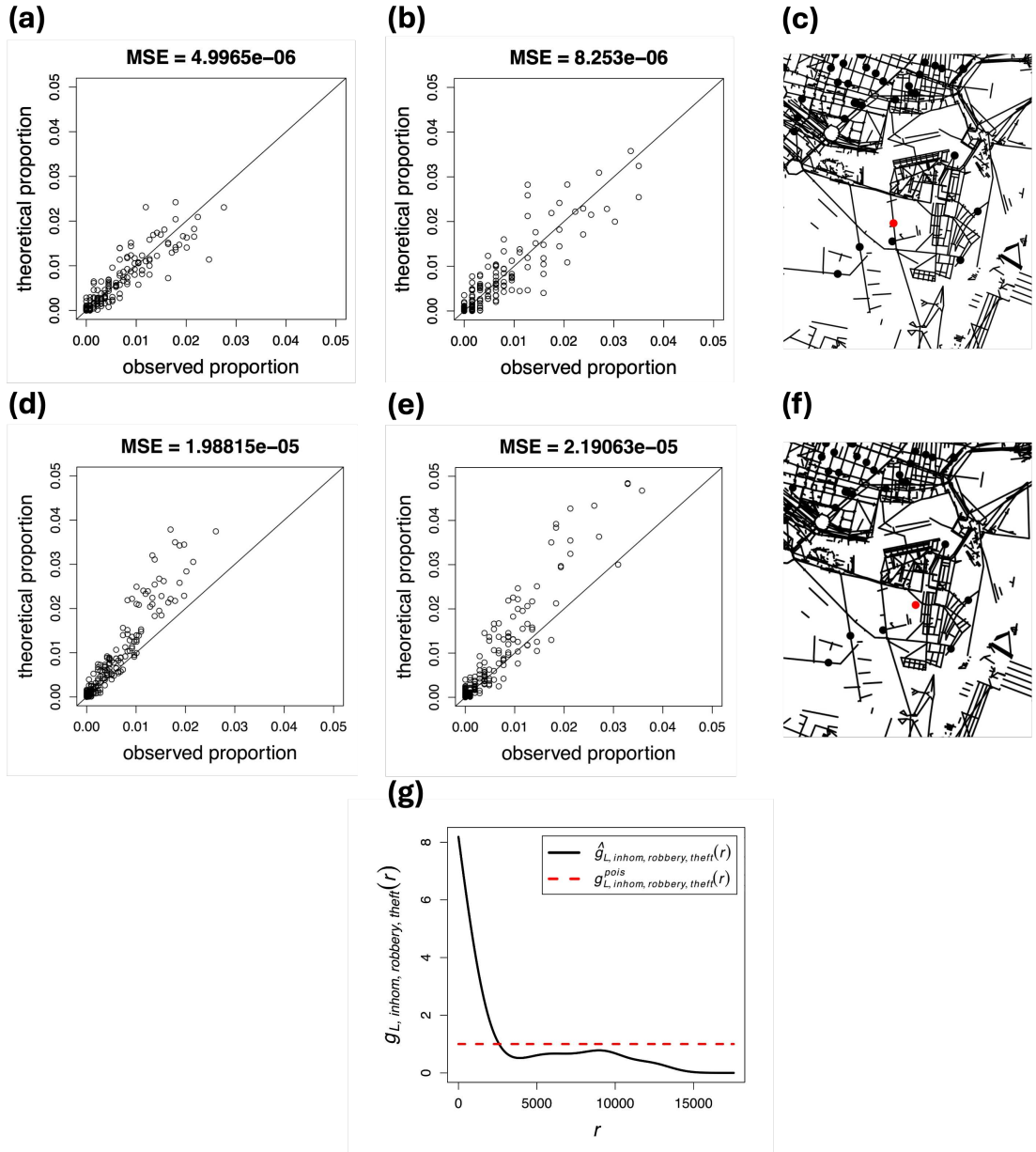


Figure 6: Model fitting comparison between the linear network DP model and the standard DP model. (a), (b) Scatter plots of (p_g^o, \hat{p}_g^t) for robbery and theft under the linear network model; (d), (e) results from the standard DP model. (c), (f) Cluster centers obtained from the linear network and standard models, respectively. Black dots represent observed crime events, and red dots indicate cluster centers. (g) Multitype pair correlation function. The black solid line represents the inhomogeneous estimate of the pair correlation function and the red dashed line represents 1, the uniform Poisson process.

DP model (Park et al., 2023), which does not account for the network structure. The standard DP model shares the same structure as our linear network DP model but uses a planar Gaussian kernel for $K_S(\cdot)$ in (4), thereby ignoring the geometry of the underlying road network. Figure 6 shows scatter plots of the estimated and observed proportions, \hat{p}_g^t and p_g^o , from both models. We observe that, for both crime types, the points from our model lie closer to the one-to-one line compared to those from the standard DP model, and the mean squared error (MSE) is also smaller. This indicates that our model more effectively captures the spatio-temporal point densities on a linear network. The limitations of the standard DP model in accounting for the road structure are also evident in the detected cluster centers. As shown in Figure 6c, our linear network model identifies clusters along the road network, whereas the standard DP model detects cluster centers in the continuous planar domain (Figure 6f). This demonstrates that our model yields more realistic and interpretable cluster locations. We fitted the model given by Equation (8) to the data described in Section 2 using Algorithm 1. The estimated parameters are summarized in Table 1.

For robbery, the space and time range parameters are about $569m$ and 0.149 (roughly 3 months and 18 days) respectively, indicating that 95% of observed points lie within approximately circles of $2 \times 569m$ and temporal intervals of 7 months. For theft, the space and time range parameters are about $552m$ and 0.141 (roughly 3 months and 12 days). Accordingly, 95% of observed points fall within circles of $2 \times 552m$ and within temporal intervals of 6 months and 24 days. With this information at hand, we can delineate the spatio-temporal structure and behavior of our crime data. These estimates align with the observation that both types of crime exhibit temporal concentration in two seasonal quarters—Q2 and Q3, which correspond to the summer and fall months. Additionally, the findings suggest that the spatial diameter of each crime cluster is approximately 1.1 kilometers, with robbery clusters being slightly more dispersed than theft clusters.

4.2 Visualization of risk boundaries

Our model is designed as an unsupervised learning approach, with the primary objective of describing spatio-temporal point patterns from data, rather than for prediction. However, based

	w_s (space)	w_t (time)
Robbery	569.322 (538.078, 596.802)	0.149 (0.142, 0.158)
Theft	551.732 (523.050, 583.479)	0.141 (0.129, 0.154)

Table 1: Posterior means and 95% HPD intervals (parentheses) of space and time range parameters for robbery and theft.

on the estimated values of w_s and w_t from past data, it is possible to construct “spatio-temporal risk boundaries”, which can be used to identify areas with a high risk of crime events over short time periods—assuming that the event distribution during such periods can be approximated by a model fitted to historical data. Such boundaries may be useful for informing social interventions to prevent crime incidents. Here, we fit the model using data from a five-month period (2018-05-15 to 2018-09-27). For robbery, the posterior means of w_s and w_t are estimated to be 567.889m and 0.05 (approximately 5 weeks), respectively. For theft, the posterior means of w_s and w_t are 524.141m and 0.047 (approximately 1 month), respectively. Figure 7 visualizes the cluster centers, their spatial risk boundaries represented by circles with radius $2 \times w_s$, and future crime events observed over the subsequent two-month period (2018-10-01 to 2018-11-30), corresponding to $2 \times w_t$. Most of the crime events fall within the risk boundaries, indicating that the model can identify areas with a high risk of crime events.

4.3 Dependence of crime incidence on amenity locations

Figure 8 illustrates the relative proportions (score) of different amenity types located within the spatial risk boundaries (i.e., $2 \times w_s$) from each cluster center. A higher proportion of a specific amenity within a cluster’s boundary suggests a potential association with the occurrence of crime events. To adjust for the overall frequency of each amenity type, we compute the following normalized score:

$$\text{Score}_k^{(j)} = \# \text{amenity}_k \text{ in cluster } j \times \left(\frac{\# \text{total amenities}}{\# \text{amenity}_k \text{ in entire area}} \right),$$

where a higher score indicates a local concentration of amenity type k in cluster j relative to its global frequency. The relative proportion of amenity types varies across clusters. Overall,

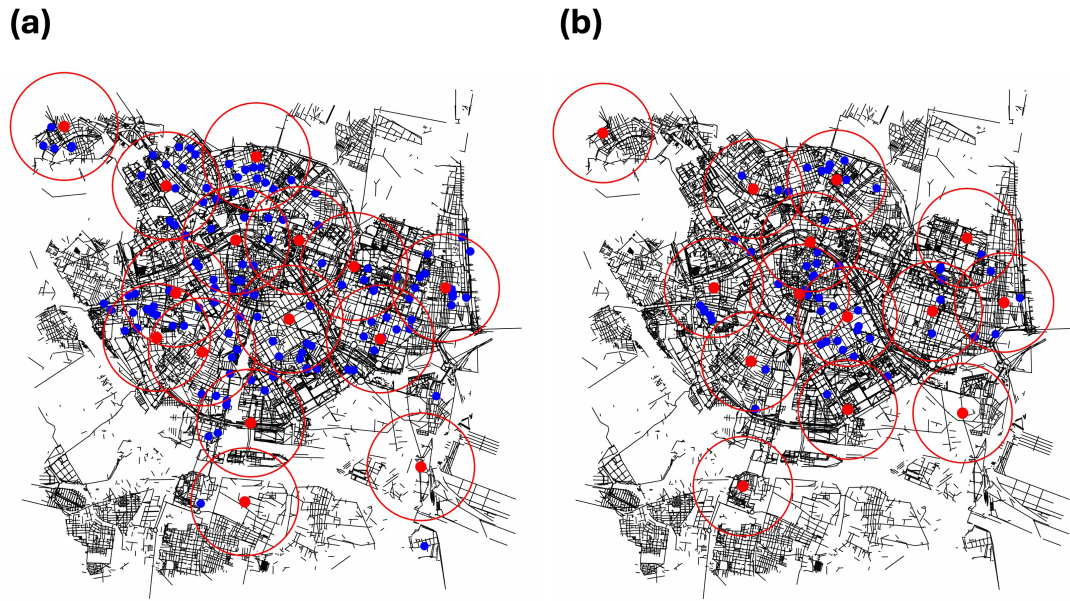


Figure 7: Risk boundaries estimated from a five-month period (2018-05-15 to 2018-09-27) for (a) robbery and (b) theft. Red circles represent risk boundaries, and red dots denote cluster centers. Blue dots indicate observed crime incidents during the subsequent two-month period (2018-10-01 to 2018-11-30).

the distribution of amenities is uneven, with the city center exhibiting a higher concentration of financial and entertainment facilities, whereas the outskirts predominantly feature eateries.

According to routine activity theory (Cohen and Felson, 1979), crime is most likely to occur where motivated offenders, suitable targets, and the absence of capable guardians converge. When integrated with research on crime specificity, which emphasizes that “even subtypes of a general crime category [may] have different causes, require different situational contexts, occur at different times and in different places, and are likely prevented by different methods” (Haberman et al., 2022, p. 432), the findings suggest that robberies in city centers are more likely to be driven by opportunities associated with financial and entertainment facilities (e.g., banks, ATMs, bars, nightclubs), whereas robberies occurring on the outskirts may be more closely linked to eateries (e.g., cafes, restaurants).

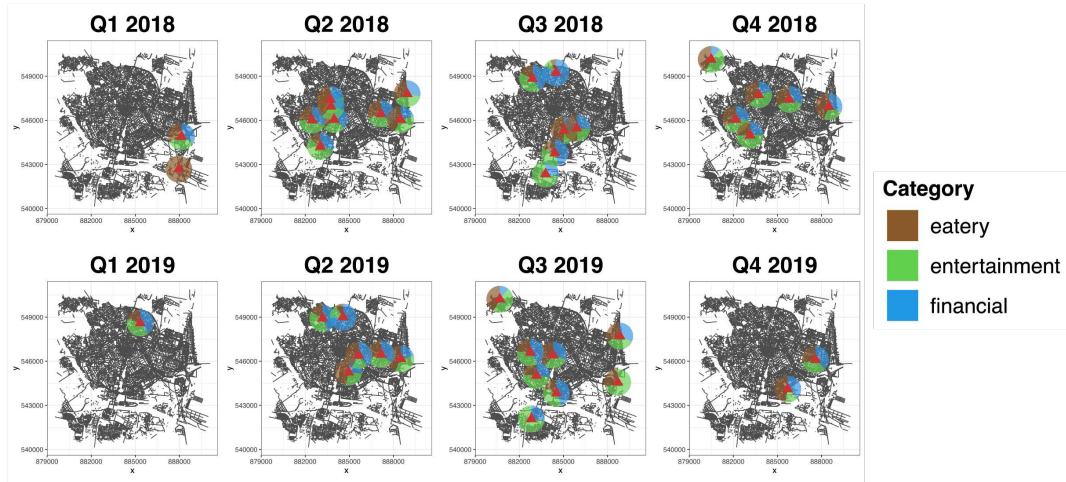
Clusters situated in the bottom-right quadrant, a coastal area, indicate that both crime categories are exclusively influenced by eateries. Note that this area of the city sits around the coast and a lake (called *Albufeira*) and is full of restaurants and open-air dining places. Thus, our

model offers additional evidence that eateries generate opportunities for crime due to high-traffic nature, elevated levels of activity and visibility, and the presence of stored cash (Brantingham and Brantingham, 1995). The bottom central area, corresponding to the downtown district, is characterized by a high concentration of entertainment-related amenities that attract pedestrians for recreational purposes, while the top central area is primarily defined by the presence of financial establishments.

Throughout the study period, entertainment venues and eateries were more prominently represented in crime clusters, compared to financial amenities. These findings align with prior research examining the relationship between land use and crime (for a review, see (Wilcox and Eck, 2011)). Specifically, commercial land use is associated with higher crime rates, residential land use with lower crime rates, and office and industrial land uses with increased property crime (Boessen and Hipp, 2015; Haberman and Ratcliffe, 2015; Kinney et al., 2008; Lee et al., 2022; Stucky and Ottensmann, 2009). However, this study only examined amenities related to commercial land use, excluding other types of land use.

We further explored the relationships between socio-economic variables and crime intensity in Valencia using Pearson correlations. We collected 14 socio-economic variables for the years 2018 and 2019 across 19 districts in Valencia. These variables include: the number of housing units; the number of employment in agriculture, manufacturing, construction, retail and service sectors, professional occupations, arts and entertainment; the number of households; the average real estate price per square meter; the total population; the number of residents born in Valencia; the number of residents born in the Horta region; the number of residents born in other regions of Spain; and the number of foreign-born residents. We then computed the average value of each variable within each district. In addition, for each district, we computed the aggregated crime intensities for both crime types over the entire study period (2018–2019). Figure 9 illustrates that the crimes examined in this study tend to be concentrated in urbanized, densely populated districts, and occur much less frequently in predominantly rural areas. Crimes that occurred in Valencia exhibit a strong positive correlation with the number of Valencia-born residents. In contrast, the numbers of residents born in Horta and other regions of Spain show relatively weaker correlations compared to other population groups. The Horta district is marked by a relatively stable population, with most residents having been born there and few newcomers

(a)



(b)

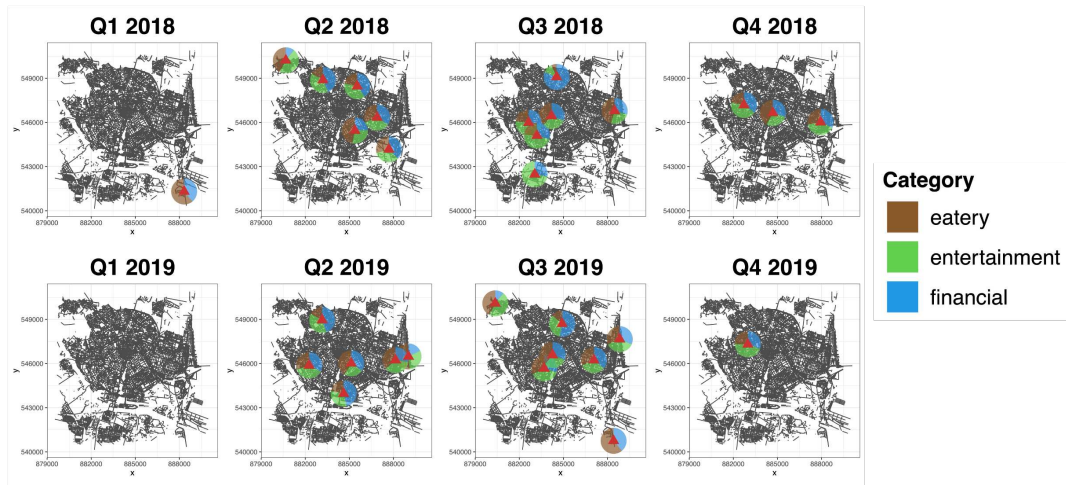


Figure 8: Amenity proportions for each cluster by quarter. Red triangles indicate detected cluster centers. The brown, green, and blue sections show proportions of eatery, entertainment, and financial amenities, respectively. (a) robbery and (b) theft.

	#houses	#agriculture	#manufacturing	#construction	#trade	#professional	#arts and ent	#households	avg property val	total pop	#Valencia born	#Horta born	#born else	#foreign-born
Robbery intensity	0.732	0.142	0.325	0.606	0.255	0.148	0.262	0.703	0.495	0.692	0.776	0.435	0.376	0.604
Theft intensity	0.653	-0.021	0.383	0.527	0.333	0.188	0.316	0.582	0.415	0.563	0.656	0.353	0.262	0.484

Figure 9: Pearson correlations between crime intensities and socio-economic variables. Blue colors indicate positive correlations, with darker shades representing stronger correlation magnitudes.

relocating for work or residence. These findings are consistent with criminological theories (Shaw and McKay, 1942; Sampson et al., 1997), which posit that crime rates tend to be higher in communities characterized by urbanization and residential instability.

4.4 Association between the two crime types

To analyze the association between the two crime types, we conduct a descriptive analysis using an inhomogeneous multitype pair correlation function (pcf) on a linear network (Baddeley et al., 2014). Specifically, after obtaining the spatial cluster centers for robbery and theft by fitting the linear DP model, we plug these centers into the inhomogeneous multitype pair correlation function to quantify how the two types of cluster centers co-locate. The inhomogeneous multitype pair correlation function is estimated as

$$\hat{\rho}^{\mathcal{L}, \text{inh}}(r) = \frac{1}{|\mathcal{L}|} \sum_{\mathbf{c}_{1,i}^s \in \mathbf{C}_1} \sum_{\mathbf{c}_{2,j}^s \in \mathbf{C}_2} \frac{\kappa(r; d_{\mathcal{L}}(\mathbf{c}_{1,i}^s, \mathbf{c}_{2,j}^s), h)}{\hat{\lambda}_1(\mathbf{c}_{1,i}^s) \hat{\lambda}_2(\mathbf{c}_{2,j}^s) M(\mathbf{v}, d_{\mathcal{L}}(\mathbf{c}_{1,i}^s, \mathbf{c}_{2,j}^s))}, \quad (9)$$

where \mathbf{C}_1 and \mathbf{C}_2 denote the spatial point processes of cluster centers for robbery and theft on the linear network \mathcal{L} , and $\mathbf{c}_{1,i}^s$ and $\mathbf{c}_{2,j}^s$ represent their i th and j th realizations, respectively. This summary statistic is used purely as a descriptive exploratory tool to assess whether the two crime-type clusters exhibit attraction ($\text{pcf} > 1$) or repulsion ($\text{pcf} < 1$) at different spatial distances along the network. In (9), $M(\mathbf{v}, d_{\mathcal{L}}(\mathbf{c}_{1,i}^s, \mathbf{c}_{2,j}^s))$ is the number of locations $\mathbf{v} \in \mathcal{L}$ that are $d_{\mathcal{L}}(\mathbf{c}_{1,i}^s, \mathbf{c}_{2,j}^s)$ away from $\mathbf{c}_{1,i}^s$ (Ang et al., 2012) in terms of the shortest-path distance. $\kappa(r; d_{\mathcal{L}}(\mathbf{c}_{1,i}^s, \mathbf{c}_{2,j}^s), h)$ denotes a planar Gaussian kernel centered with the center $d_{\mathcal{L}}(\mathbf{c}_{1,i}^s, \mathbf{c}_{2,j}^s)$ and the bandwidth h , which is determined using a Scott's rule (Scott, 2015). We use the convolution kernel estimator

(Rakshit et al., 2019b) to obtain $\hat{\lambda}_1(\cdot)$ and $\hat{\lambda}_2(\cdot)$. Specifically, for each crime type $m \in \{1, 2\}$, corresponding to robbery and theft, the intensity at the arbitrary point $\mathbf{u} \in \mathcal{L}$ is

$$\hat{\lambda}_m(\mathbf{u}) = \sum_{\mathbf{c}_{m,l}^s \in \mathbf{C}_m} \frac{\kappa(\mathbf{u}; \mathbf{c}_{m,l}^s, w_m)}{c_{\mathcal{L}}(\mathbf{u})},$$

where κ is a planar Gaussian kernel with a smoothing bandwidth w_m and $c_{\mathcal{L}}(\mathbf{u}) = \int_{\mathcal{L}} \kappa(\mathbf{v}; \mathbf{u}, w_m) d_1 \mathbf{v}$ is a correction term to consider the network geometry. The bandwidth parameter was chosen according to Scott's rule (Scott, 2015).

We computed a multitype pairwise correlation function between spatial cluster centers from the two crime types by using the `linearpcfcross.inhom` function from the `spatstat.linnet` package. From Figure 8, we observe that the centers of the two crimes (red triangles) are close in Q3 of 2018 and Q2, Q3 of 2019. Indeed, the pcf plot (see Figure 6g) takes values exceeding 1 at certain spatial distances ($r < 2500$), indicating an attraction tendency. In contrast, we observe that the centers of the two crimes have a repulsive pattern in Q4 of 2019 (Figure 8), and the computed pcf values drop below 1 at around $r > 2500$. These results indicate that robbery and theft crime clusters are more concentrated in the fall when both peak and become more dispersed in other seasons with lower crime activity.

To study the association between the two crime types, we also fit a spatio-temporal conditional autoregressive (CAR) model (Lee et al., 2018) by regressing the log-transformed robbery intensity on the log-transformed theft intensity, where both intensities are obtained using the convolution kernel estimator (Rakshit et al., 2019b). For the spatio-temporal regression, we use a 64×64 spatial grid, where each pixel is associated with an estimated intensity value at 8 time points corresponding to quarterly intervals over a two-year period. We provide details of the spatio-temporal CAR model and its implementation in the supplementary material. We observe that the regression coefficient is significantly positive, indicating that theft has a positive impact on robbery. Furthermore, autocorrelation parameters are statistically significant, suggesting the presence of spatial and temporal autocorrelation in the relationship between the two crime types.

5 Discussion

In this paper, we have proposed a Bayesian spatio-temporal point process model on a linear network. With a DP prior, the model can detect unobserved space-time cluster centers of crime incidence over the street network. From the detected cluster centers, we study the association between amenities and crime events, which provides interesting criminological research findings. Furthermore, we have estimated spatio-temporal intensities that can describe the pattern of crime events in the city. We use the computationally efficient convolution kernel estimator (Rakshit et al., 2019b) in our model to account for the geometrical structure of the street network. We have also assessed the performance of the model by comparing the theoretical and empirical densities and observed that our model fits well. To our knowledge, this is the first attempt to consider the Bayesian framework for the point process analysis on a linear network.

There are several caveats to be further considered in future research. An excessive number of cluster centers may lead to overfitting, but this issue can be mitigated through appropriate prior specification, as implemented in our work. The hyperparameter in the stick-breaking process can be set to discourage an overly large number of non-empty clusters (Reich and Bondell, 2011). In addition, specifying an informative prior on the range parameter can discourage the model from producing cluster centers with too small ranges (Park et al., 2023). Alternatively, the model could be extended to a supervised learning framework by splitting the data into training and test sets to improve out-of-sample generalization. In this study, we fitted the model to two crime types separately and analyzed the correlation between their cluster centers. Our model can be extended to a bivariate point process setting. Recently, Briz-Redón and Mateu (2023) proposed a mechanistic bivariate point process over the planar space, assuming that the current crime event is affected by different crime types in the past. Another direction is to model the crime events as a marked point process that has information about the crime type. Several Bayesian approaches have been developed to model data with geographic locations and categorical marks (Jiao et al., 2021; Quick et al., 2015).

Research on multitype marked point processes on linear networks is still in an early stage, although recent studies have made progress. For example, Eckardt and Moradi (2024) reviewed and extended mark-related summaries to linear networks, highlighting that methodological de-

velopments for marked inhomogeneous processes on linear networks remain limited. Other contributions include extensions of summary characteristics to function-valued marks (Eckardt et al., 2025a), the use of compositional data analysis for marked spatial point processes (Eckardt et al., 2025b), and the proposal of graph-based summaries such as the graph mark variogram to capture complex point patterns (Eckardt et al., 2024). These works mainly focus on summary characteristics rather than proposing new models. Incorporating such frameworks into our model would be an interesting extension. There have been several proposals to study the relation between multiple types of events over time. For example, Taddy (2010) developed an autoregressive mixture model with an autoregressive Beta stick-breaking process to study spatio-temporal relationships between extreme and non-extreme crimes. Eckardt et al. (2021) proposed partial point process characteristics to capture direct dependencies in multivariate marked spatio-temporal point processes. Extending such work to our application would require kernel estimators that account for network geometry, which would be computationally intensive. We therefore consider this direction as part of our future work.

Supplementary Material

Supplementary materials available online contain full conditionals for the MCMC algorithm and grid computation details.

Acknowledgement

This work was supported by the National Research Foundation of Korea (RS-2025-00513129, RS-2025-00523567, RS-2023-00217705) and the New Faculty Startup Fund from Seoul National University (326-20240027). J. Mateu has been funded by research projects CIAICO/2022/191 from Generalitat Valenciana and PID2022-141555OB-I00 from the Spanish Ministry of Science and Innovation. The authors are grateful to Mehdi Moradi for providing useful sample code and advice.

Data Availability Statement

The datasets and source code can be downloaded from <https://github.com/SujeongLee/stdplinet>.

Conflict of Interest Statement

The authors declare that they have no conflicts of interest.

References

- Ang, Q. W., Baddeley, A., and Nair, G. (2012). Geometrically Corrected Second Order Analysis of Events on a Linear Network, with Applications to Ecology and Criminology. *Scandinavian Journal of Statistics*, 39(4):591–617.
- Baddeley, A., Jammalamadaka, A., and Nair, G. (2014). Multitype point process analysis of spines on the dendrite network of a neuron. *Journal of the Royal Statistical Society Series C: Applied Statistics*, 63(5):673–694.
- Baddeley, A., Nair, G., Rakshit, S., McSwiggan, G., and Davies, T. M. (2021). Analysing point patterns on networks—A review. *Spatial Statistics*, 42:100435.
- Baddeley, A., Rubak, E., and Turner, R. (2015). *Spatial Point Patterns: Methodology and Applications with R*. Chapman and Hall/CRC Press, London.
- Baddeley, A., Turner, R., Møller, J., and Hazelton, M. (2005). Residual Analysis for Spatial Point Processes (with Discussion). *Journal of the Royal Statistical Society Series B: Statistical Methodology*, 67(5):617–666.
- Binder, D. A. (1978). Bayesian cluster analysis. *Biometrika*, 65(1):31–38.
- Block, R. (2000). Gang Activity and Overall Levels of Crime: A New Mapping Tool for Defining Areas of Gang Activity Using Police Records. *Journal of Quantitative Criminology*, 16(3):369–383.
- Boessen, A. and Hipp, J. R. (2015). Close-ups and the scale of ecology: Land uses and the geography of social context and crime. *Criminology*, 53(3):399–426.
- Brantingham, P. and Brantingham, P. (1995). Criminality of place: Crime generators and crime attractors. *European Journal of Criminal Policy and Research*, 3:5–26.
- Brantingham, P. J., Carter, J., MacDonald, J., Melde, C., and Mohler, G. (2021a). Is the recent surge in violence in American cities due to contagion? *Journal of Criminal Justice*, 76:101848.
- Brantingham, P. J., Yuan, B., and Herz, D. (2021b). Is Gang Violent Crime More Contagious than Non-Gang Violent Crime? *Journal of Quantitative Criminology*, 37:953–977.

- Brantingham, P. L., Brantingham, P. J., Vajihollahi, M., and Wuschke, K. (2009). Crime analysis at multiple scales of aggregation: A topological approach. In Weisburd, D., Bernasco, W., and Bruinsma, G. J. N., editors, *Putting crime in its place*, chapter 4, pages 87–107. Springer, New York.
- Briz-Redón, Á. and Mateu, J. (2023). A mechanistic bivariate point process model for crime pattern analysis. *Stat*, 12(1):e537.
- Chastain, B., Qiu, F., and Piquero, A. R. (2016). Crime Theory Evaluation Using Simulation Models of Residential Burglary. *American Journal of Criminal Justice*, 41:814–833.
- Chiu, S.-T. (1991). Bandwidth selection for kernel density estimation. *The Annals of Statistics*, 19(4):1883–1905.
- Cohen, L. E. and Felson, M. (1979). Social change and crime rate trends: A routine activity approach. *American Sociological Review*, 44(4):588–608.
- Cohn, E. G. (1990). Weather and crime. *The British Journal of Criminology*, 30(1):51–64.
- Cressie, N. and Wikle, C. K. (2011). *Statistics for Spatio-Temporal Data*. John Wiley & Sons.
- Dahl, D. B. (2006). Model-Based Clustering for Expression Data via a Dirichlet Process Mixture Model. *Bayesian inference for gene expression and proteomics*, 4:201–218.
- Deckard, M. and Schnell, C. (2023). The Temporal (in)Stability of Violent Crime Hot Spots Between Months and The Modifiable Temporal Unit Problem. *Crime & Delinquency*, 69(6-7):1312–1335.
- Dong, Z., Mateu, J., and Xie, Y. (2024). Spatio-Temporal-Network Point Processes for Modeling Crime Events with Landmarks. *arXiv preprint arXiv:2409.10882*.
- D’Angelo, N., Adelfio, G., Abbruzzo, A., and Mateu, J. (2022). Inhomogeneous spatio-temporal point processes on linear networks for visitors’ stops data. *The Annals of Applied Statistics*, 16(2):791–815.

- D'Angelo, N., Adelfio, G., and Mateu, J. (2023). Local inhomogeneous second-order characteristics for spatio-temporal point processes occurring on linear networks. *Statistical Papers*, 64(3):779–805.
- D'Angelo, N., Payares, D., Adelfio, G., and Mateu, J. (2024). Self-exciting point process modelling of crimes on linear networks. *Statistical Modelling*, 24(2):139–168.
- Eckardt, M., Comas, C., and Mateu, J. (2025a). Summary characteristics for multivariate function-valued spatial point process attributes. *International Statistical Review*, 93(1):150–178.
- Eckardt, M., Ghorbanpour, F., and Särkkä, A. (2024). Second-order characteristics for spatial point processes with graph-valued marks. *arXiv preprint arXiv:2410.16903*.
- Eckardt, M., González, J. A., and Mateu, J. (2021). Graphical modelling and partial characteristics for multitype and multivariate-marked spatio-temporal point processes. *Computational Statistics & Data Analysis*, 156:107139.
- Eckardt, M. and Moradi, M. (2024). Marked Spatial Point Processes: Current State and Extensions to Point Processes on Linear Networks. *Journal of Agricultural Biological and Environmental Statistics*, 29:346–378.
- Eckardt, M., Myllymäki, M., and Greven, S. (2025b). On spatial point processes with composition-valued marks. *arXiv preprint arXiv:2501.16049*.
- Farrell, G. and Pease, K. (1994). CRIME SEASONALITY: Domestic Disputes and Residential Burglary in Merseyside 1988-90. *The British Journal of Criminology*, 34(4):487–498.
- Gilardi, A., Borgoni, R., and Mateu, J. (2024). A nonseparable first-order spatiotemporal intensity for events on linear networks: An application to ambulance interventions. *The Annals of Applied Statistics*, 18(1):529–554.
- Groff, E. R. (2007). Simulation for Theory Testing and Experimentation: An Example Using Routine Activity Theory and Street Robbery. *Journal of Quantitative Criminology*, 23:75–103.

- Groff, E. R., Ratcliffe, J. H., Harberman, C. P., Sorg, E. T., Joyce, N. M., and Taylor, R. B. (2015). Does what police do at hot spots matter? The Philadelphia policing tactics experiment. *Criminology*, 53(1):23–53.
- Haberman, C. P., Clutter, J. E., and Lee, H. (2022). A robbery is a robbery is a robbery? Exploring crime specificity in official police incident data. *Police Practice and Research*, 23(4):429–443.
- Haberman, C. P. and Ratcliffe, J. H. (2015). Testing for temporally differentiated relationships among potentially criminogenic places and census block street robbery counts. *Criminology*, 53(3):457–483.
- Haberman, C. P., Sorg, E. T., and Ratcliffe, J. H. (2018). The Seasons They Are a Changin’: Testing for Seasonal Effects of Potentially Criminogenic Places on Street Robbery. *Journal of Research in Crime and Delinquency*, 55(3):425–459.
- Hessellund, K. B., Xu, G., Guan, Y., and Waagepetersen, R. (2022). Semiparametric Multinomial Logistic Regression for Multivariate Point Pattern Data. *Journal of the American Statistical Association*, 117(539):1500–1515.
- Hipp, J. R., Curran, P. J., Bollen, K. A., and Bauer, D. J. (2004). Crimes of Opportunity or Crimes of Emotion? Testing Two Explanations of Seasonal Change in Crime. *Social Forces*, 82(4):1333–1372.
- Instituto Nacional de Estadística (2025). Tourist movement on borders, Comunitat Valenciana, Base data.
- Ishwaran, H. and James, L. F. (2001). Gibbs Sampling Methods for Stick-Breaking Priors. *Journal of the American Statistical Association*, 96(453):161–173.
- Jiao, J., Hu, G., and Yan, J. (2021). A Bayesian marked spatial point processes model for basketball shot chart. *Journal of Quantitative Analysis in Sports*, 17(2):77–90.
- Johnson, S. D. (2008a). Repeat burglary victimisation: a tale of two theories. *Journal of Experimental Criminology*, 4:215–240.

- Johnson, S. D. (2008b). Repeat burglary victimization: a tale of two theories. *Journal of Experimental Criminology*, 4:215–240.
- Kim, Y.-A. and Wo, J. C. (2022). Seasonality and Crime in Orlando Neighbourhoods. *The British Journal of Criminology*, 62(1):124–144.
- Kinney, J. B., Brantingham, P. L., Wuschke, K., Kirk, M. G., and Brantingham, P. J. (2008). Crime Attractors, Generators and Detractors: Land Use and Urban Crime Opportunities. *Built Environment*, 34(1):62–74.
- Kottas, A. and Sansó, B. (2007). Bayesian mixture modeling for spatial Poisson process intensities, with applications to extreme value analysis. *Journal of Statistical Planning and Inference*, 137(10):3151–3163.
- Lee, D., Rushworth, A., and Napier, G. (2018). Spatio-Temporal Areal Unit Modeling in R with Conditional Autoregressive Priors Using the CARBayesST Package. *Journal of Statistical Software*, 84(9):1–39.
- Lee, Y.-J., O, S.-H., and Eck, J. E. (2022). Why Your Bar Has Crime But Not Mine: Resolving the Land Use and Crime-Risky Facility Conflict. *Justice Quarterly*, 39(5):1009–1035.
- Lima, R. (2023). Hawkes Processes Modeling, Inference, and Control: An Overview. *SIAM Review*, 65(2):331–374.
- Loeffler, C. and Flaxman, S. (2018). Is Gun Violence Contagious? A Spatiotemporal Test. *Journal of Quantitative Criminology*, 34(4):999–1017.
- Mark Padgham, Bob Rudis, Robin Lovelace, and Maëlle Salmon (2017). osmdata. *Journal of Open Source Software*, 2(14):305.
- McDowall, D., Loftin, C., and Pate, M. (2012). Seasonal Cycles in Crime, and Their Variability. *Journal of Quantitative Criminology*, 28:389–410.
- McSwiggan, G., Baddeley, A., and Nair, G. (2017). Kernel Density Estimation on a Linear Network. *Scandinavian Journal of Statistics*, 44(2):324–345.

- Medvedovic, M. and Sivaganesan, S. (2002). Bayesian infinite mixture model based clustering of gene expression profiles. *Bioinformatics*, 18(9):1194–1206.
- Mohler, G. (2014). Marked point process hotspot maps for homicide and gun crime prediction in Chicago. *International Journal of Forecasting*, 30(3):491–497.
- Mohler, G. O., Short, M. B., Brantingham, P. J., Schoenberg, F. P., and Tita, G. E. (2011). Self-Exciting Point Process Modeling of Crime. *Journal of the American Statistical Association*, 106(493):100–108.
- Møller, J. and Waagepetersen, R. P. (2003). *Statistical Inference and Simulation for Spatial Point Processes*. CRC press.
- Moradi, M. M. and Mateu, J. (2020). First-and Second-Order Characteristics of Spatio-Temporal Point Processes on Linear Networks. *Journal of Computational and Graphical Statistics*, 29(3):432–443.
- Okabe, A. and Sugihara, K. (2012). *Spatial Analysis Along Networks: Statistical and Computational Methods*. Wiley.
- Park, J., Schoenberg, F. P., Bertozzi, A. L., and Brantingham, P. J. (2021). Investigating Clustering and Violence Interruption in Gang-Related Violent Crime Data Using Spatial-Temporal Point Processes With Covariates. *Journal of the American Statistical Association*, 116(536):1674–1687.
- Park, J., Yi, S., Chang, W., and Mateu, J. (2023). A spatio-temporal Dirichlet process mixture model for coronavirus disease-19. *Statistics in Medicine*, 42(30):5555–5576.
- Quick, H., Holan, S. H., Wikle, C. K., and Reiter, J. P. (2015). Bayesian marked point process modeling for generating fully synthetic public use data with point-referenced geography. *Spatial Statistics*, 14:439–451.
- R Core Team (2022). *R: A Language and Environment for Statistical Computing*. R Foundation for Statistical Computing, Vienna, Austria.

- Rakshit, S., Baddeley, A., and Nair, G. (2019a). Efficient Code for Second Order Analysis of Events on a Linear Network. *Journal of Statistical Software*, 90(1):1–37.
- Rakshit, S., Davies, T., Moradi, M. M., McSwiggan, G., Nair, G., Mateu, J., and Baddeley, A. (2019b). Fast Kernel Smoothing of Point Patterns on a Large Network using Two-dimensional Convolution. *International Statistical Review*, 87(3):531–556.
- Reich, B. J. and Bondell, H. D. (2011). A Spatial Dirichlet Process Mixture Model for Clustering Population Genetics Data. *Biometrics*, 67(2):381–390.
- Reinhart, A. (2018). A Review of Self-Exciting Spatio-Temporal Point Processes and Their Applications. *Statistical Science*, 33(3):299–318.
- Ripley, B. D. (1976). The second-order analysis of stationary point processes. *Journal of Applied Probability*, 13(2):255–266.
- Sampson, R. J., Raudenbush, S. W., and Earls, F. (1997). Neighborhoods and Violent Crime: A Multilevel Study of Collective Efficacy. *Science*, 277(5328):918–924.
- Santitissadeekorn, N., Short, M. B., and Lloyd, D. J. B. (2018). Sequential data assimilation for 1D self-exciting processes with application to urban crime data. *Computational Statistics and Data Analysis*, 128:163–183.
- Scott, D. W. (2015). *Multivariate density estimation: theory, practice, and visualization*. John Wiley & Sons.
- Sethuraman, J. (1994). A constructive definition of Dirichlet priors. *Statistica Sinica*, pages 639–650.
- Shaw, C. R. and McKay, H. D. (1942). *Juvenile delinquency and urban areas*. University of Chicago Press.
- Song, J., Spicer, V., and Brantingham, P. (2013). The edge effect: Exploring high crime zones near residential neighborhoods. In *2013 IEEE International Conference on Intelligence and Security Informatics*, pages 245–250.

- Stucky, T. D. and Ottensmann, J. R. (2009). Land use and violent crime. *Criminology*, 47(4):1223–1264.
- Taddy, M. A. (2010). Autoregressive Mixture Models for Dynamic Spatial Poisson Processes: Application to Tracking Intensity of Violent Crime. *Journal of the American Statistical Association*, 105(492):1403–1417.
- Taylor-Rodríguez, D., Kaufeld, K., Schliep, E. M., Clark, J. S., and Gelfand, A. E. (2017). Joint Species Distribution Modeling: Dimension Reduction Using Dirichlet Processes. *Bayesian Analysis*, 12(4):939–967.
- van Dijk, J., Nieuwbeerta, P., and Larsen, J. J. (2022). Global Crime Patterns: An Analysis of Survey Data from 166 Countries Around the World, 2006–2019. *Journal of Quantitative Criminology*, 38:793–827.
- Weisburd, D. (2018). Hot Spots of Crime and Place-Based Prevention. *Criminology & Public Policy*, 17(1):5–25.
- Wilcox, P. and Eck, J. E. (2011). Criminology of the unpopular: Implications for policy aimed at payday lending facilities. *Criminology & Public Policy*, 10(2):473–482.
- Zhang, X., Liu, L., Lan, M., Song, G., Xiao, L., and Chen, J. (2022). Interpretable machine learning models for crime prediction. *Computers, Environment and Urban Systems*, 94:101789.
- Zhuang, J. and Mateu, J. (2019). A semiparametric spatiotemporal Hawkes-type point process model with periodic background for crime data. *Journal of the Royal Statistical Society Series A: Statistics in Society*, 182(3):919–942.

Supplementary Materials for A Spatio-Temporal Dirichlet Process Mixture Model on Linear Networks for Crime Data

Sujeong Lee, Won Chang, Jorge Mateu, Heejin Lee, and Jaewoo Park

January 21, 2026

1 The Bayesian hierarchical model structure

$$\text{Likelihood: } \prod_{i=1}^N \left[\sum_{\forall j \text{ non-empty}} q_j K_S(\mathbf{x}_i; \mathbf{c}_j^s, w_s) K_T(t_i; c_j^t, w_t) \right]$$

$$\text{Dirichlet process prior: } g_i \sim \text{Categorical}(q_1, \dots, q_M)$$

$$q_j = U_1 \text{ for } j = 1 \text{ and } q_j = U_j \prod_{m=1}^{j-1} (1 - U_m) \text{ for } j = 2, \dots, M$$

$$U_1, \dots, U_M \stackrel{\text{iid}}{\sim} \text{Beta}(1, b_u)$$

$$b_u \sim \text{Gamma}(1, c)$$

$$\text{Parameter prior: } w_s \sim N(\mu_s, 400) I_{[100, 1000]}(w_s)$$

$$w_t \sim N(\mu_t, 400) I_{[0, \infty)}(w_t)$$

$$\text{Cluster prior: } \mathbf{c} \sim \frac{1}{|\Delta| \mathcal{T}}$$

2 Full conditionals for MCMC

1. The conditional distribution of range parameters (w_s, w_t) :

$$\begin{aligned} \pi(w_s, w_t | \text{others}) &\propto \prod_{i=1}^N f((\mathbf{x}_i, t_i) | w_s, w_t) \pi(w_s) \pi(w_t) \\ &\propto \prod_{i=1}^N \left[\sum_{\forall j \text{ non-empty}} q_j K_S(\mathbf{x}_i; \mathbf{c}_j^s, w_s) K_T(t_i; c_j^t, w_t) \right] \times \pi(w_s) \pi(w_t). \end{aligned}$$

2. The conditional distribution of membership variable g_i :

$$\pi(g_i | \text{others}) = \text{Categorical}(\tilde{q}_{i1}, \dots, \tilde{q}_{iM})$$

where

$$\tilde{q}_{ij} \propto q_j K_S(\mathbf{x}_i; \mathbf{c}_j^s, w_s) K_T(t_i; c_j^t, w_t)$$

for $j = 1, \dots, M$.

3. The conditional distribution of space-time cluster centers (\mathbf{c}_j^s, c_j^t) :

$$\pi((\mathbf{c}_j^s, c_j^t) | \text{others}) \propto \prod_{\forall i | g_i=j} q_j K_S(\mathbf{x}_i; \mathbf{c}_j^s, w_s) K_T(t_i; c_j^t, w_t) \times \frac{1}{|\Delta| \mathcal{T}}$$

for $j = 1, \dots, M$.

4. The conditional distribution of U_j :

$$\pi(U_j|\text{others}) = \text{Beta} \left(1 + \sum_{i=1}^N \mathbb{1}\{g_i = j\}, b_u + \sum_{i=1}^N \mathbb{1}\{g_i > j\} \right).$$

5. The conditional distribution of b_u :

$$\pi(b_u|\text{others}) = \text{Gamma} \left(M - 1 + a, c - \sum_{j=1}^{M-1} \log(1 - U_j) \right),$$

where $a=1$, $c=1$ and $1/4$.

3 Grid computation details

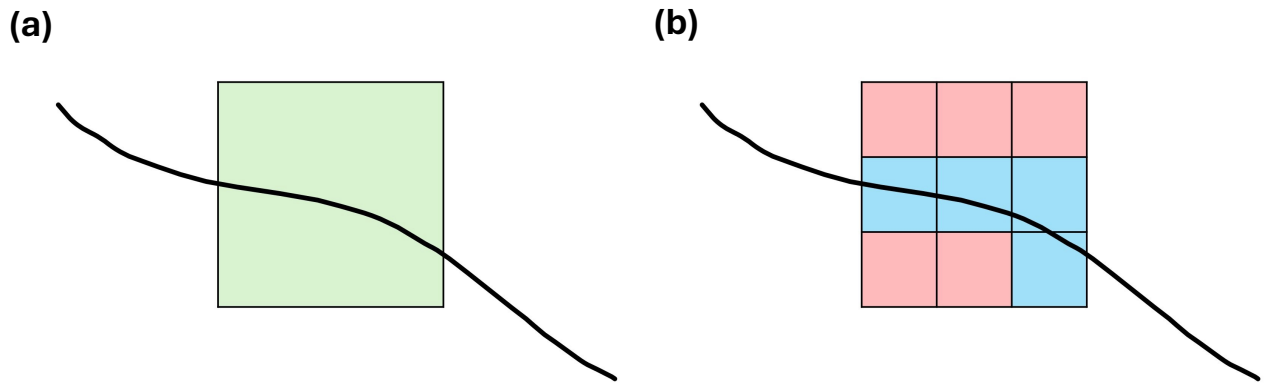


Figure 1: (a) Grid and subgrid (b) covering the road network. Among the cubes belonging to the subgrid, only the part containing the road network (blue colors) was used in the aggregation step.

4 Residual maps for model validation

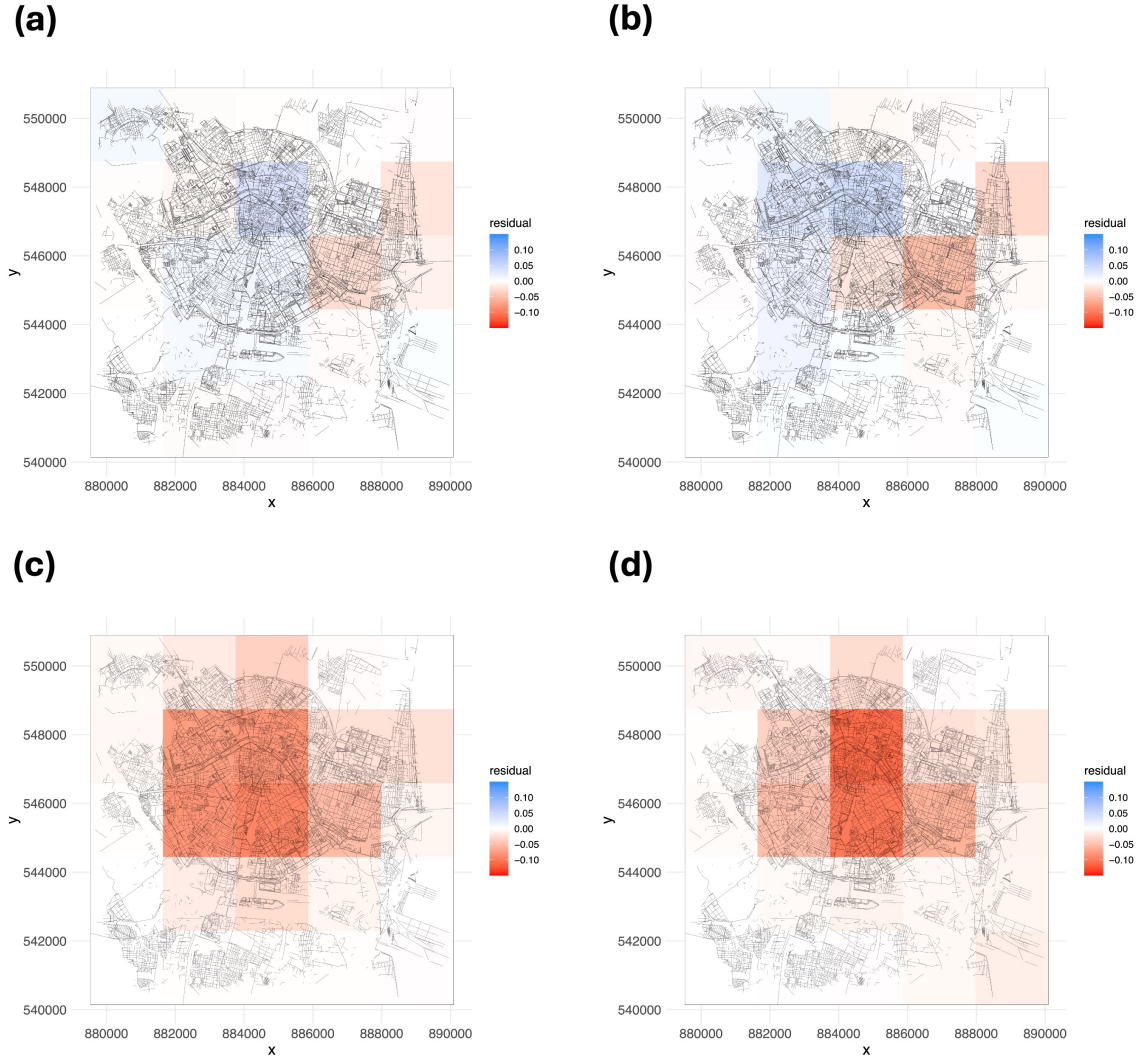


Figure 2: (a), (b) Residual maps of robbery and theft from the linear network DP model. (c), (d) Residual maps of robbery and theft from the standard DP model.

We compute the residuals over a $G = 5 \times 5 \times 10$ grid, which is the same grid used for comparing observed and theoretical proportions. For visualization over the two-dimensional spatial domain, we aggregate the residuals by summing over the temporal grid points. Figure 2 shows that the residuals from the linear network model are more distributed around zero, indicating a better fit compared to the standard DP model.

5 Spatio-temporal conditional autoregressive model

Let y_{kt} and x_{kt} denote the log-transformed robbery intensity and log-transformed theft intensity at location k and time t , respectively. We use a 64×64 spatial grid, where each pixel is associated with an estimated intensity value at eight time points corresponding to quarterly intervals over two years. Therefore, the indices range are $k = 1, \dots, 4096$ and $t = 1, \dots, 8$. We fit a spatio-temporal conditional autoregressive (CAR) model

[Lee et al., 2018] using the `ST.CARar` function from the `CARBayesST` package, defined as follows:

$$\begin{aligned}
 y_{kt} &\sim \mathcal{N}(\beta_0 + x_{kt}\beta_1 + \phi_{kt}, \nu^2) \\
 \phi_t | \phi_{t-1} &\sim \text{N}(\rho_T \phi_{t-1}, \tau^2 \mathbf{Q}(\mathbf{W}, \rho_S)^{-1}) \\
 \phi_1 &\sim \text{N}(\mathbf{0}, \tau^2 \mathbf{Q}(\mathbf{W}, \rho_S)^{-1}) \\
 \tau^2 &\sim \text{Inverse-Gamma}(a, b) \\
 \rho_S, \rho_T &\sim \text{Uniform}(0, 1),
 \end{aligned}$$

where $\mathbf{W} = (w_{kj})$ is a $K \times K$ adjacency matrix, and ϕ_{kt} is a spatio-temporal random effect at location k and time t . The vector $\phi_t = (\phi_{1t}, \dots, \phi_{4096t})$ represents the spatial random effects at time t . The precision matrix is defined as $\mathbf{Q}(\mathbf{W}, \rho_S) = \rho_S[\text{diag}(\mathbf{W}\mathbf{1}) - \mathbf{W}] + (1 - \rho_S)\mathbf{I}$, where $\mathbf{1}$ is a $K \times 1$ vector of ones, and \mathbf{I} is the $K \times K$ identity matrix. ν^2 denotes the error variance, τ^2 is the variance of the spatio-temporal random effects, and ρ_S and ρ_T are the spatial and temporal autocorrelation coefficients. We run the MCMC algorithm for 400,000 iterations to fit the model, and the results are summarized in Table 1. We observe that the regression coefficient β_1 is significantly positive, indicating that theft has a positive impact on robbery. Furthermore, both ρ_S and ρ_T are statistically significant, suggesting the presence of spatial and temporal autocorrelation in the relationship between the two crime types.

Parameter	Mean	2.5%	97.5%
β_0	-9.1445	-9.1805	-9.0994
β_1	0.1277	0.1246	0.1316
ν^2	0.0001	0.0001	0.0001
τ^2	0.0996	0.0978	0.1015
ρ_S	0.9999	0.9999	1.0000
ρ_T	0.6906	0.6801	0.7012

Table 1: Posterior means and 95% HPD intervals of the parameters.

References

Duncan Lee, Alastair Rushworth, and Gary Napier. Spatio-Temporal Areal Unit Modeling in R with Conditional Autoregressive Priors Using the `CARBayesST` Package. *Journal of Statistical Software*, 84(9):1–39, 2018.